1 General

Rene 95, which was developed by General Electric Co., is one of the strongest nickel-base superalloys for highly stressed rotating gas-turbine engine components such as compressor discs, turbine discs, cooling plates, and related hardware operating at temperatures up to about 1200F. Although it was originally produced as cast and wrought products, since about 1980 it has been processed primarily by powder-metallurgy (P/M) techniques either as hot isostatically pressed (HIP) products or as isothermally forged components produced from HIP or hot-extruded powder compacts. The following are advantages of powder-metal processing of Rene 95: (1) production of more complex shapes with less chemical segregation to adversely affect mechanical properties; (2) better machinability and less machining required; (3) fewer manufacturing steps; and (4) raw-material savings of up to 50 percent, which is a vital factor in view of the scarce, expensive alloying elements used in Rene 95.

Optimum properties are achieved by solution, quench, and age-hardening heat treatment, which produces a combination of gamma-prime [Ni_3(Al, Ti, Cb)] precipitation strengthening and solid-solution strengthening by addition of chromium, cobalt, molybdenum, and tungsten. Minor boron and zirconium additions impart beneficial grain-boundary effects to enhance creep resistance. (Refs. 1, 2, 4, 7, 9, 11, 12, 25)

1.1 Commercial Designation

Rene 95

1.2 Alternate Designations

None

1.3 Specifications

No government, ASTM, AMS or other types of consensus specifications have been published for the alloy. General Electric (G.E.) has developed its own company specifications or product requirements. (Ref. 30)

1.4 Composition

1.4.1 *[Table]* G.E. specified composition.

Ni	
13	Cr
8	Co
3.5	Mo
3.5	Cb
3.5	Al
3.5	W
2.5	Ti
0.06	C
0.05	Zr
0.01	B

1.5 Heat Treatment

Rene 95 develops optimum properties in the age-hardened condition, which requires solution-plus-aging heat treatment. The important heat-treat variables are solution temperature and time, cooling rate from the solution temperature, and age-hardening temperatures and times. Numerous combinations of these variables have been used with reasonable success on Rene 95 products, but, apparently, no widespread consensus or standard had emerged for an optimum treatment.

Most sources prefer solution treatments of one hour at temperatures ranging from 2000 to 2100F, which is slightly below the gamma-prime solvus of about 2135F. Cooling from the solution temperature ranges from oil quench to air cool. However, many sources now prefer a salt-bath quench at elevated temperature, usually 1000F; this type of quench provides a delicate balance between possible low properties if the quench is too slow and cracking if the quench is too rapid.

Age hardening is accomplished by either a single or a double elevated-temperature exposure followed by air cooling. The most widely used aging treatments are as follows: single exposure, 1400F 16 hours; double exposure, 1600F 1 hour plus 1200F either 16 or 24 hours. G.E. prefers the double exposure for as-HIP products and the single exposure for HIP plus forged products. (Refs. 1, 2, 4, 8, 25, 30, 32)

1.5.1 *[Figure]* Variations in tensile properties at room temperature resulting from variations in solution-plus-age heat treatment.

1.5.2 *[Figure]* Variations in tensile properties at 1200F resulting from variations in solution-plus-age heat treatment.

1.5.3 *[Table]* Effects of variations in solution-plus-age heat treatment on creep and rupture properties at 1200F.

1.6 Hardness

1.7 Forms and Conditions Available

Available primarily as powder-metal products—as-HIP, HIP plus hot forged, and extruded plus hot forged. Formerly, but no longer regularly, available in conventional wrought forms such as billets, bars, plate, and forgings. Normally used in the solution-treated-and-aged conditions. (See Section 1.5) (Ref. 31)

1.8 Melting and Casting Practice

Vacuum-induction melting followed by vacuum-arc remelting have been used for the production of cast and wrought products and of pre-alloyed forms subsequently used to make atomized powders. Also in some instances, electroslag remelt has been used instead of vacuum arc. Vacuum-induction melting is used in the production of atomized powders. (Refs. 14, 17, 20, 30)

This section produced with the support of NASA-Lewis Research Center.

1.9 Special Consideration

Satisfactory performance of gas-turbine discs and related hardware requires good low-cycle fatigue properties and resistance to crack propagation, particularly at temperatures in the vicinity of 1200F. Consequently, much of the research and development on P/M Rene 95 has involved studies of these properties and various factors that affect them. Three factors that have been found to be quite significant are the environment, defects, and grain size. Specific test results showing the effects of such variables are given in Sections 3.4 and 3.5.

1.9.1 Environment. A number of studies have determined that low-cycle fatigue life of P/M Rene 95 decreases while both fatigue- and creep-crack growth rates increase with increasing concentrations of environmental oxygen at elevated temperatures. For example, degradation of these properties tends to be quite severe in air environments as compared with vacuum of 5×10^{-5} torr or better. Even the small concentration of 1-2 ppm of oxygen in argon environments has a significantly adverse effect. In other words, the fatigue and creep behavior of this alloy are pronounced functions of the partial pressure of oxygen. A possible mechanism for this phenomenon is stress- and deformation-assisted oxygen diffusion ahead of the crack tip. The degradation of resistance to fatigue-crack growth and to low-cycle fatigue failure with decreasing frequency and with cyclic hold times in air or in argon, as shown in Section 3.5, is probably a manifestation, primarily, of the susceptibility of the alloy to oxygen-induced damage rather than of fatigue-creep interaction. (Refs. 5, 6, 7, 8, 13, 27, 28)

1.9.2 Defects. The fatigue life of Rene 95 powder-metal products is adversely affected by defects, such as inclusions and porosity, which provide points of premature fatigue-crack initiation. Inclusions are usually ceramic oxides or carbides that originate, for example, from the vacuum-induction-melting crucible, pouring tundish, or atomizing nozzle used for the production of the powder; other possible sources are contaminated melting stock and careless handling of the powder prior to the HIP process. The most common source of porosity is argon-gas entrapped in powder particles during atomization or possibly introduced during hot isostatic pressing as a result of inadequate outgassing and container evacuation and sealing procedures. (Refs. 7, 12, 18, 24, 25, 30, 32, 34)

One controlled study of the effects of variations in defect size (both inclusions and porosity) and location on low-cycle fatigue life shows that larger defects and surface locations intensify the detrimental effects. The less severe effect of internal defects is ascribed to the absence of environmental interactions, particularly with oxygen. (Refs. 12, 25)

1.9.2.1 *[Figure]* Effects of defect size (cross-sectional area) and location on low-cycle fatigue life at 1000F.

1.9.3 Grain Size. Fine grain sizes in Rene 95, like most other metals, tend to provide optimum combinations of strength, ductility, and resistance to fatigue-crack initiation. However, larger grain sizes provide better resistance to fatigue-crack propagation as well as to creep. Consequently, fine-grain Rene 95 products tend to be superior in strength, in resistance to fatigue-crack initiation, and in total low-cycle fatigue life but inferior in resistance to fatigue-crack growth as compared with similar coarse-grain products. (See Figures 3.5.2.6, 3.5.2.7, 3.5.3.9 - 3.5.3.12)

Generally, HIP Rene 95 products have a fine uniform grain size of ASTM No. 8 or finer. The powder products that are forged after consolidation can be produced either with a uniform recrystallized fine grain size of ASTM No. 10-11 or with a dual grain size consisting of a "necklace" of fine recrystallized grains of ASTM No. 8 or finer surrounding larger elongated unrecrystallized grains coarser than ASTM No. 6. The formation of the dual "necklace" grain structure, which normally provides better ductility and creep properties, requires careful control of thermal-mechanical processing. For example, one source recommends HIP temperatures of 2200F, forging reductions of 50-60 percent at 2025F, and solution temperature of 2000F. Apparently, lower HIP temperatures, greater forging reductions, and higher solution temperatures are conducive to the uniform fine-grain structures. The dual "necklace" grain structure was also preferred for many conventional wrought-from-cast-ingot products. (Refs. 10, 25, 30, 31, 32, 33, 36)

1.9.4 Comparisons with IN 718 (Code 4103), which is representative of conventional wrought-from-ingot superalloys used in jet engines up to about 1200F, show Rene 95 to be superior in tensile and creep strength. Although IN 718, in general, has slightly better fatigue-crack-growth resistance, P/M Rene 95 products provide better low-cycle-fatigue life, apparently because of superior resistance to crack initiation. (Ref. 32)

1.9.4.1 *[Table]* Comparison of the tensile, stress-rupture, and cyclic rupture properties of P/M Rene 95 and IN 718 alloys.

1.9.4.2 *[Figure]* Comparison of low-cycle fatigue life as a function of total cyclic strain for Rene 95 and IN 718 at 1200F and cyclic frequency of 0.33 Hz.

1.9.4.3 *[Figure]* Comparison of low-cycle fatigue life as a function of total cyclic strain for Rene 95 and IN 718 at 1200F and with a 15-minute hold time at maximum cyclic tensile strain.

1.9.4.4 *[Figure]* Comparison of fatigue crack growth rates for Rene 95 and IN 718 at 1200F and cyclic frequency of 0.33 Hz.

2 Physical Properties and Environmental Effects

Only a limited number of the thermal, physical, and corrosion properties of Rene 95 can be reliably established; consequently, many of the property categories called for in this section are not available. For the vacant categories, corresponding data in the chapter on Rene

80, Code 4214, which is a somewhat similar sister alloy, may provide the best available approximations for the Rene 95 properties.

2.1 Thermal Properties

2.1.1 Melting Range.

2.1.2 Phase Changes.

The phases normally present in Rene 95 are a gamma-solid-solution matrix of chromium, cobalt, molybdenum, and tungsten in nickel; minor amounts of carbides of columbium, titanium, tungsten, and chromium; and substantial amounts of gamma prime, which consists of intermetallic compounds of nickel with aluminum, titanium, and columbium. During solution heat treatment, which is normally somewhat below the solvus temperature of approximately 2135F, most of the gamma prime is dissolved in the matrix. The undissolved gamma prime is useful in preventing excessive grain growth. With proper quenching, most of the gamma prime remains in solution until numerous small dispersed particles are precipitated throughout the matrix during the age-hardening treatment normally at temperatures in the range 1200 to 1400F. (Refs. 2, 8, 10, 19, 25, 30, 32, 33)

2.1.2.1 Time-temperature-transformation diagrams

2.1.3 Thermal Conductivity.

2.1.4 Thermal Expansion.

2.1.4.1 *[Figure]* Coefficient of thermal expansion from 77F to 1400F.

2.1.5 Specific Heat.

2.1.6 Thermal Diffusivity.

2.2 Other Physical Properties

2.2.1 Density. 0.297 - 0.299 lb/cu. in. (Refs. 30, 31, 36)

2.2.2 Electrical Properties.

2.3.2 Magnetic Properties.

2.2.4 Emittance.

2.2.5 Damping Capacity.

2.3 Chemical Environments

2.3.1 General Corrosion.

2.3.1.1 Oxidizing environments. See Section 1.9.1.

2.3.2 Stress Corrosion.

2.4 Nuclear Environments

3 Mechanical Properties

3.1 Specified Mechanical Properties

3.1.1 *[Table]* G.E. minimum mechanical-property requirements for P/M HIP products in section thicknesses up to 1.8 in.

3.1.2 *[Table]* G.E. minimum mechanical-property requirements for P/M HIP plus forged products in section thicknesses up to 1.8 in.

3.2 Mechanical Properties at Room Temperature

3.2.1 Tension Stress-strain Diagrams and Tensile Properties

3.2.1.1 *[Figure]* Tensile properties at room temperature of Rene 95 formed by various methods.

3.2.2 Compressive Stress-strain Diagrams and Compressive Properties.

3.2.3 Impact.

3.2.4 Bending.

3.2.5 Tension and Shear.

3.2.6 Bearing.

3.2.7 Stress Concentration.

3.2.7.1 Notch Properties.

3.2.7.2 Fracture Toughness.

3.2.8 Combined Loading.

3.3 Mechanical Properties at Various Temperatures

3.3.1 Tension Stress-strain Diagrams and Tensile Properties.

3.3.1.1 *[Table]* Tensile properties at room temperature and 1200F of P/M HIP, P/M HIP + forged, and wrought Rene 95.

3.3.1.2 *[Table]* Tensile properties at 1005 and 1200F of P/M HIP, P/M extruded + forged, and wrought Rene 95.

3.3.1.3 *[Table]* Results of tensile tests at room temperature and 1200F on 150 P/M HIP jet-engine discs.

3.3.1.4 *[Table]* Tensile-property ranges for a total of 18 tests, both at room temperature and 1200F, on six HIP + forged P/M products.

3.3.1.5 *[Table]* Tensile properties at 1000F resulting from variations in atomizing gas, powder mesh size, HIP cycle, and heat treatment.

3.3.1.6 *[Table]* Tensile properties at 1000F resulting from variations in HIP cycle, and heat treatment.

3.3.1.7 *[Figure]* Tensile properties at 1200F resulting from various forming methods.

3.3.1.8 *[Figure]* Effects of elevated temperatures up to 1200F on tensile properties of two rear shafts.

3.3.1.9 *[Figure]* Effects of elevated temperatures up to 1200F on tensile properties compressor discs.

3.3.1.10 *[Figure]* Effects of different production processes on tensile properies at temperatures up to 1400F.

3.3.1.11 *[Figure]* Effects of elevated temperatures up to 1200F on tensile properties turbine disc.

3.3.2 Compression Stress-strain Diagrams and Compression Properties.

3.3.3 Impact.

3.3.5 Torsion and Shear.

3.3.6 Bearing.

3.3.7 Stress Concentration.

3.3.7.1 Notch Properties.

3.3.7.1.1 *[Figure]* Comparison of ultimate tensile strength and notched tensile strength (K_t = 2) of rear shafts at room temperatures up to 1200F.

3.3.7.2 Fracture Toughness.

3.3.8 Combined Loading.

3.4 Creep and Creep Rupture Properties

3.4.1 *[Figure]* Stress-rupture properties at 1200F and 150 ksi of Rene 95 formed by various methods.

3.4.2 *[Table]* Mean results of stress-rupture and creep tests on specimens from 150 P/M HIP jet-engine discs.

3.4.3 *[Table]* Stress-rupture life of six HIP plus forged powder products (2 tests each) at 1200F and 150 ksi.

3.4.4 *[Table]* Creep-rupture properties of forgings at 1200F.

3.4.5 *[Figure]* Stress-rupture properties of rear shafts at 1100 to 1300F.

3.4.6 *[Figure]* Stress-rupture properties of compressor discs at 1100 to 1300F.

3.4.7 *[Figure]* Creep crack growth rate as a function of stress intensity factor at 1200F in air and in purified argon.

3.4.8 *[Figure]* Creep crack growth rate as a function of stress intensity factor at 1400F in air and in purified argon.

3.4.9 *[Figure]* Creep crack growth rate as a function of stress intensity factor at 1300F in air and in purified argon.

3.4.10 *[Figure]* Creep crack growth rate as a function of stress intensity factor at 1200F in air and in vacuum.

3.5 Fatigue Properties

3.5.1 Conventional High-Cycle Fatigue.

3.5.2 Low-Cycle Fatigue.

3.5.2.1 *[Figure]* Effects of holding two minutes at maximum cyclic tensile strain on low-cycle fatigue life of P/M HIP Rene 95 as a function of total cyclic strain at 1200F and 1325F in argon.

3.5.2.2 *[Figure]* Effects of holding 15 minutes at maximum cyclic tensile strain on low-cycle fatigue life of P/M HIP Rene 95 as a function of total cyclic strain at 1200F in air.

3.5.2.3 *[Figure]* Effects of holding 15 minutes at maximum cyclic tensile strain on low-cycle fatigue life of P/M HIP Rene 95 as a function of total cyclic strain at 1200F in air.

3.5.2.4 *[Figure]* Low-cycle fatigue life at 1200F as a function of total cyclic strain for HIP and HIP plus forged Rene 95

3.5.2.5 *[Figure]* Low-cycle fatigue life of HIP plus forged Rene 95 as a function of total cyclic strain at 1200F with two different strain ratios (minimum cyclic strain/maximum cyclic strain).

3.5.2.6 *[Figure]* Effects of different forming methods on low-cycle fatigue life as a function of total cyclic strain at 1005F.

3.5.2.7 *[Figure]* Effects of different forming methods on low-cycle fatigue life as a function of total cyclic strain at 1200F.

3.5.2.8 *[Figure]* Effects of variations in cyclic hold times on the low-cycle fatigue life of forgings as a function of total cyclic strain at 1200F.

3.5.3 Fatigue Crack Propagation.

3.5.3.1 *[Figure]* Fatigue crack growth rates at room temperature in air and in vacuum.

3.5.3.2 *[Figure]* Fatigue crack growth rates at 1200F and 1335F in argon.

3.5.3.3 *[Figure]* Fatigue crack growth rates at 1200F in air and in argon.

3.5.3.4 *[Figure]* Fatigue crack growth rates at 1200F in vacuum and in argon.

3.5.3.5 *[Figure]* Effects of variations in cycling rate on fatigue crack growth rates at 1200F in argon.

3.5.3.6 *[Figure]* Effects of variations in cycling rate on fatigue crack growth rates at 1200F in air and in vacuum.

3.5.3.7 *[Figure]* Effects of holding 15 minutes at maximum cyclic tensile stress on the fatigue crack growth rates at 1200F in air.

3.5.3.8 *[Figure]* Effects of holding two minutes at maximum cyclic tensile stress on the fatigue crack growth rates at 1200F in argon.

3.5.3.9 *[Figure]* Effects of different forming methods and grain sizes on fatigue crack growth rates at 1005F in air at 0.33 Hz.

3.5.3.10 *[Figure]* Effects of different forming methods and grain sizes on fatigue crack growth rates at 1200F in air at 0.33 Hz.

3.5.3.11 *[Figure]* Effects of different forming methods and grain sizes on fatigue crack growth rates at 1200F in vacuum at 0.33 Hz.

3.5.3.12 *[Figure]* Effects of different forming methods and grain sizes on fatigue crack growth rates at 1200F in air with cycling at 0.33 Hz plus two minute hold time at maximum cyclic stress.

3.5.3.13 *[Figure]* Effects of variations in powder mesh size and processing parameters on crack growth rates in axial fatigue at 1000F, 0.33 Hz and R = 0.05, in air.

3.5.3.14 *[Figure]* Effects of different R values (min/max cyclic stress) on near threshold fatigue crack growth rates of wrought Rene 95 at 75F in air at 25 Hz.

3.6 Elastic Properties

3.6.1 Poisson's Ratio (See Code 4214, Figure 3.061 for best estimate)

3.6.2 Modulus of Elasticity.

3.6.2.1 *[Figure]* Modulus of elasticity at temperatures from 75F to 1500F.

3.6.3 Modulus of Rigidity.

3.6.4 Tangent Modulus.

3.6.5 Secant Modulus.

4 Fabrication

4.1 Forming

4.1.1 HIP Products. Typically, the following processing steps are involved in the forming of Rene 95 HIP powder-metal parts:

a. Production of the powder by atomization, in which the alloy is vacuum-induction melted in a non-reactive crucible and then poured into the reservoir of an atomizing nozzle, all under vacuum. As the liquid metal leaves the nozzle, a high-velocity inert gas stream (usually argon) impinges on it. The argon breaks the liquid into small droplets, which solidify to powder as they fall into a collection chamber.

b. Screening to remove oversize and nonspherical particles that would interfere with packing uniformity during hot isostatic pressing.

c. Blending and mixing of powder from several atomization batches to ensure homogeneity of particle size. Use of various particle sizes from -60 to -270 mesh have been reported; -60 and -150 are commonly used sizes. One major investigation (Ref. 30) reported "no major effects on properties was observed for variations in Rene 95 powder particle size ranges of -60, -60 + -150, and -150 mesh."

d. Container fabrication, which involves shaping containers from low-carbon or stainless steel sheet with cavities closely resembling the final product. These preshaped containers can be hydroformed, spun, or die formed and are usually joined by gas-tungsten-arc welding. Alternatively, complex near net shapes can be made using ceramic containers made by a method similar to the lost-wax investment-casting process.

e. Filling and sealing the container with powder by gravity flow through a tubular system, possibly assisted by vibrating the container, after which the fill stem is crimped off and welded shut under vacuum.

f. Hot isostatic pressing (compaction) which occurs when the sealed container is heated and pressed in an autoclave causing the powder to coalesce and form a solid approaching theoretical density. Typical compaction parameters are 15 ksi and 2050 to 2200F for a minimum of two hours resulting in material of essentially theoretical density.

g. Removal of container, usually by machining or chemical processing.

h. Semi-finish machining if necessary.

i. Heat treatment to achieve optimum mechanical properties (see Section 1.5).

j. Ultrasonic inspection for internal integrity and by fluorescent penetrant for surface flaws.

k. Machining to final dimensions if necessary. (Refs. 1, 2, 4, 10, 13, 14, 24, 25, 30)

4.1.2 HIP Plus Forged P/M Products. For HIP-plus-forged products, the above sequence (Section 4.1.1) applies with the addition of forging after HIP either before or after removal of the container. Forging temperatures are normally about 2000 to 2050F; forming reductions up to 60 percent and sometimes more are feasible. (Refs. 2, 13, 30)

4.1.3 Compacted, Extruded, and Forged P/M Products. A description of this method by one source is as follows: (1) compact -150 mesh powder to roughly 90 percent density at 1830F in a blanked extrusion press; (2) extrude at 1960F to a reduction of 7:1 in cross section; (3) section to desired lengths and isothermally forge to desired shape at 2010F. The forged shapes can subsequently be heat treated and finish machined as needed. (Ref. 16)

4.1.4 Conventionally Cast and Forged Products. Descriptions, from two sources, of the formation of turbine-disc type forgings begin with vacuum-induction melting and vacuum-arc remelt to produce an ingot 9-in. in diameter, which was homogenized at about 2000F, three hours, and air cooled. Pancakes of appropriate thickness taken from the ingot were forged in the range 2000 to 2080F to reduce them to 40-50 percent above final thickness, followed by a recrystallization anneal at 2125F, one hour, and cooling to 1650F at a rate greater than 170F per hour and then air cooling. Final forging to the desired dimensions was than applied at 1975 to 2025F, after which the forgings were ready for finish machining, if necessary, and solution-and-age heat treatment. (Refs. 17, 34)

4.2 Machining and Grinding

Rene 95 is tough and difficult to machine prior to age-hardening; it is more difficult to machine in the age-hardened condition, which has a machinability rating of 8-10 percent of that of AISI B112 steel. The use of a sulfur-base cutting fluid is recommended. The alloy is not considered machinable with high-speed steel cutting tools. Rather, micro-grain carbide tools are normally used. Also, borazon tools have been found

to be costs effective in some instances such as light turning cuts less than 0.020 in. deep. (Refs. 4, 30, 31)

4.3 Joining

4.4 Surface Treating

Table 1.4.1 G.E. specified composition (Ref. 30)

Alloy	Rene 95	
Element (percent)	Minimum	Maximum
Carbon	0.04	0.09
Manganese	—	0.15
Silicon	—	0.20
Sulfur	—	0.015
Phosphorus	—	0.015
Chromium	12.00	14.00
Cobalt	7.00	9.00
Molybdenum	3.30	3.70
Iron	—	0.50
Tantalum	—	0.20
Columbium	3.30	3.70
Zirconium	0.03	0.07
Titanium	2.30	2.70
Aluminum	3.30	3.70
Boron	0.006	0.015
Tungsten	3.30	3.70
Oxygen	—	0.015
Nitrogen	—	0.005
Hydrogen	—	0.001
Nickel	Balance	

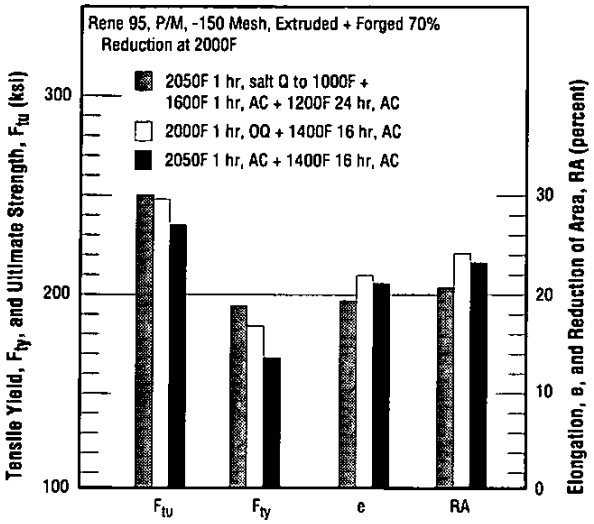

Figure 1.5.1 Variations in tensile properties at room temperature resulting from variations in solution-plus-age heat treatment (Ref. 25)

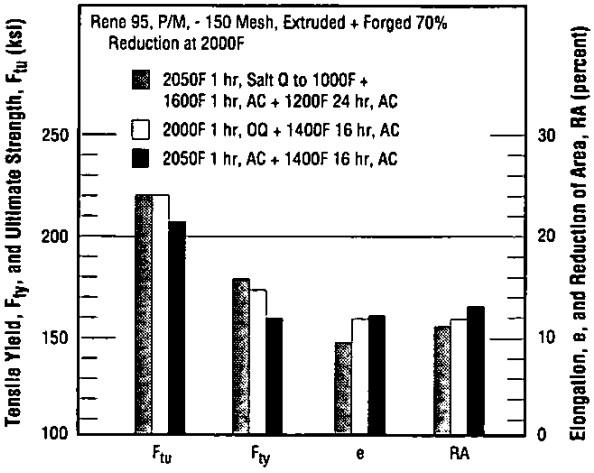

Figure 1.5.2 Variations in tensile properties at 1200F resulting from variations in solution-plus-age heat treatment (Ref. 25)

Table 1.5.3 Effects of variations in solution-plus-age heat treatment on creep and rupture properties at 1200F (Ref. 25)

Alloy	Rene 95		
Form	P/M -150 Mesh, Extruded Plus Forged 70% Reduction at 2000F		
Heat Treatment	2050F 1 hr, Q to 1000F + 1600F 1 hr, AC + 1200F 24 hr, AC	2000F 1 hr, OQ + 1400F 16 hr, AC	2050F 1 hr, AC + 1400F 16 hr, AC
Temperature (F)	1200	1200	1200
Stress (ksi)	150	150	150
Rupture Time (hr)	85.2	107.7	18.6
Stress (ksi)	123	123	123
% Creep at 50 hours	0.02	0.02	0.16

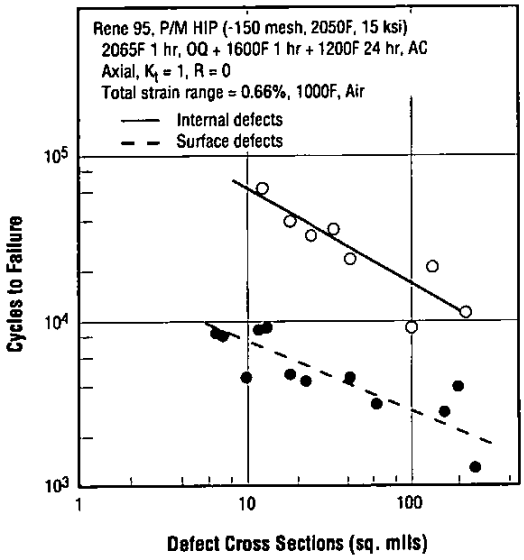

Figure 1.9.2.1 Effects of defect size (cross-sectional area) and location on low-cycle fatigue life at 1000F (Refs. 12, 25)

Table 1.9.4.1 Comparison of the tensile, stress-rupture, and cyclic rupture properties of P/M Rene 95 and IN 718 alloys (Ref. 32)

Alloy	Rene 95		Rene 95		IN 718	
Form	P/M HIP		P/M HIP + Forge		Forging	
Condition	Solution-Treated and Aged					
Temperature (F)	75	1200	75	1200	75	1200
Tensile:						
F_{ty} (ksi)	176.1	162.4	171	162.6	169.2	141.0
F_{tu} (ksi)	237.3	219.6	236	214.6	210.9	168.5
e (percent)	16.2	16.4	18.4	12.8	15.8	20.8
RA (percent)	15.2	17.3	22.7	14.2	23.9	43.8
Stress Rupture:						
Stress (ksi)		150		150		100
Rupture Time (hr)		69.6		298.1		254.5
e (percent)		—		2.2		17.3
Cyclic Rupture: [a]						
Maximum Stress (ksi)		145		145		
Cycles to Rupture		630		571.5		
Time to Rupture (hr)		19.2		18.1		

[a] Cycles consisted of loading to maximum tensile stress in 10 seconds, holding 90 seconds and unloading in 10 seconds.

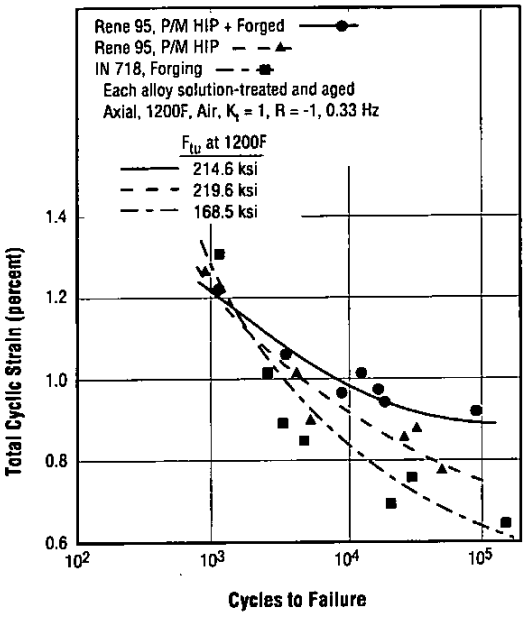

Figure 1.9.4.2 Comparison of low-cycle fatigue life as a function of total cyclic strain for Rene 95 and IN 718 at 1200F and cyclic frequency of 0.33 Hz (Ref. 32)

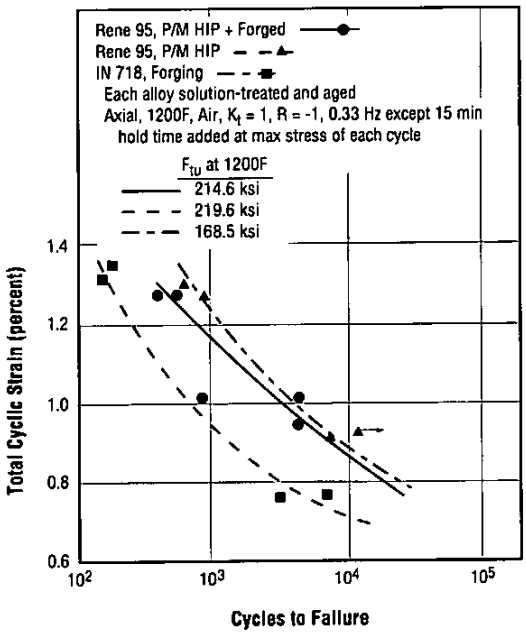

Figure 1.9.4.3 Comparison of low-cycle fatigue life as a function of total cyclic strain for Rene 95 and IN 718 at 1200F and with a 15-minute hold time at maximum cyclic tensile strain (Ref. 32)

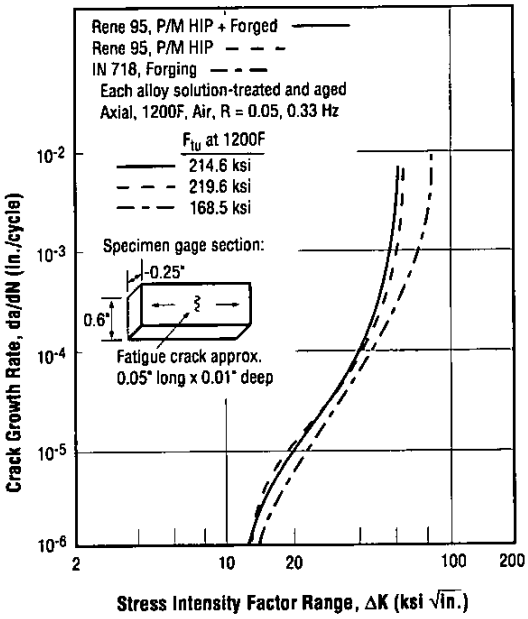

Figure 1.9.4.4 Comparison of fatigue crack growth rates for Rene 95 and IN 718 at 1200F and cyclic frequency of 0.33 Hz (Ref. 32)

Note: A separate investigation indicates that crack-growth rates determined with this type of specimen (known as K_b bar) are approximately two times faster than those obtained with the compact tension, C(T), type specimen. (Ref. 33) On the other hand, Reference 32 states that "by simulating directly the component stresses and crack sizes that might result from fatigue loading, the (K_b bar) test data are directly applicable to (jet-engine) components."

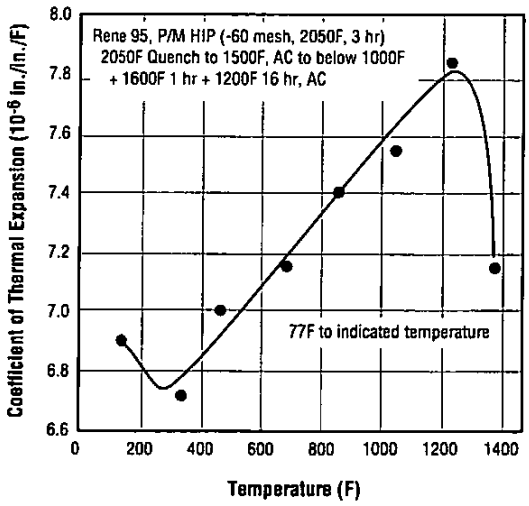

Figure 2.1.4.1 Coefficient of thermal expansion from 77F to 1400F (Ref. 30)

Table 3.1.1 G.E. minimum mechanical-property requirements for P/M HIP products in section thicknesses up to 1.8 in. (Ref. 30)

Alloy	Rene 95		
Form	P/M HIP (-60 Mesh, 2050F, 15 ksi, 2 hr minimum)		
Condition	2050F 1 hr, Quench to 1500F, AC to below 1000F + 1600F 1 hr + 1200F 16 hr, AC		
Temperature (F)	Property[a]		Minimum
75	F_{ty} (ksi)		166
	F_{tu} (ksi)		217
	e (percent)		10
	RA (percent)		12
1200	F_{ty} (ksi)		151
	F_{tu} (ksi)		198
	e (percent)		8
	RA (percent)		10
1200	Stress Rupture at 140 ksi	Time (hr)	25
		e (percent)	2

[a] Properties for sections greater than 1.8-inch thick as-heat-treated shall be as agreed upon between purchaser and vendor.

Table 3.1.2 G.E. minimum mechanical-property requirements for P/M HIP plus forged products in section thicknesses up to 1.8 in. (Ref. 30)

Alloy	Rene 95			
Form	P/M HIP (-60 Mesh, 2200F, 15 ksi, 2 hr minimum) plus forged 50 - 60% reduction at 2025F			
Condition	2000F 1-2 hr, oil or salt quench to maximum of 1000F + 1400F 16 hr, AC			
Temperature (F)	Property		Minimum	
			t < 1.4 in.	1.4 ≤ t ≤ 1.8[a]
75	F_{ty} (ksi)		175	171
	F_{tu} (ksi)		224	221
	e (percent)		10	10
	RA (percent)		12	12
1200	F_{ty} (ksi)		162	158
	F_{tu} (ksi)		207	204
	e (percent)		8	8
	RA (percent)		10	10
1200	Stress Rupture at 150 ksi	Time (hr)	25	25
		e (percent)	2	2

[a] Properties for sections greater than 1.8-inch thick as-heat-treated shall be as agreed upon between purchaser and vendor.

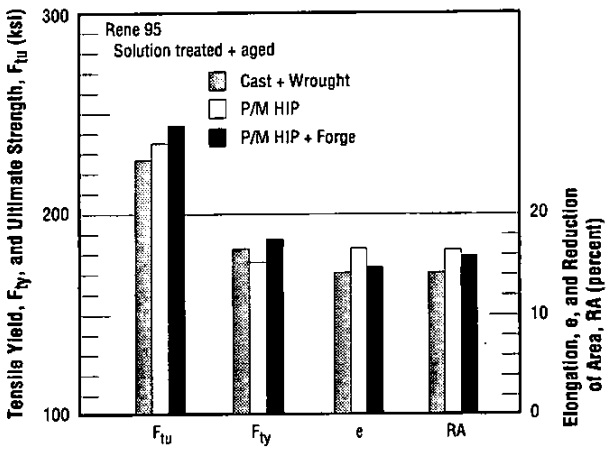

Figure 3.2.1.1 Tensile properties at room temperature of Rene 95 formed by various methods (Ref. 24)

Table 3.3.1.1 Tensile properties at room temperature and 1200F of P/M HIP, P/M HIP + forged, and wrought Rene 95 (Ref. 3)

Alloy	Rene 95				
Condition	2100F 1 hr, 1000F Q + 1600F 1 hr + 1200F 24 hr, AC				
Form[a]	Temperature (F)	F_{ty} (ksi)	F_{tu} (ksi)	e (percent)	RA (percent)
P/M HIP	75	176	237	15	16
P/M HIP + Forged		171	236	23	18
Cast + Wrought		166	208	12	10
P/M HIP	1200	162	220	17	16
P/M HIP + Forged		163	215	14	13
Cast + Wrought		153	186	10	8

[a] HIP = hot isostatically pressed at 2050F, 15 ksi, 3 hours.

Table 3.3.1.2 Tensile properties at 1005F and 1200F of P/M HIP, P/M extruded + forged, and wrought Rene 95 (Ref. 16)

Alloy	Rene 95				
Condition	2050F 1 hr, AC + 1400F 8 hr, AC[a]				
Form[b]	Temperature (F)	F_{ty} (ksi)	F_{tu} (ksi)	e (percent)	RA (percent)
P/M HIP	1005	162.4	226.3	16.6	19.1
P/M Extruded + Forged		165.3	226.3	18.6	19.6
Cast + Rolled Plate		136.3	175.5	8.6	14.3
P/M HIP	1200	159.5	217.6	13.8	13.4
P/M Extruded + Forged		165.3	217.6	12.4	16.2
Cast + Rolled Plate		134.7	181.3	9.0	13.0

[a] Prior to solution-and-age heat treatment, the wrought plate was homogenized at 2225F one hour and air cooled.

[b] Average grain sizes in microns: HIP, 5; extruded + forged, 8; wrought plate, 150.

Table 3.3.1.3 Results of tensile tests at room temperature and 1200F on 150 P/M HIP jet-engine discs (Ref. 14)

Alloy	Rene 95		
Form	P/M HIP Jet-Engine Discs		
Condition	Solution Treated, Quenched and Aged		
Property	Temperature (F)	Mean	Standard Deviation
F_{ty} (ksi)	75	176.9	3.5
F_{tu} (ksi)		239.4	2.8
e (percent)		17.2	1.9
RA (percent)		20.5	1.8
F_{ty} (ksi)	1200	165.2	5.4
F_{tu} (ksi)		220.1	4.9
e (percent)		13.8	4.1
RA (percent)		16.5	3.3

Table 3.3.1.4 Tensile-property ranges for a total of 18 tests, both at room temperature and 1200F, on six HIP + forged P/M products (Ref. 2)

Alloy	Rene 95			
Form[a]	P/M HIP + Forged			
Condition	1650F 24 hr, AC + 2000F 1 hr, OQ + 1400F 16 hr, AC			
Temperature (F)	F_{ty} (ksi)	F_{tu} (ksi)	e (percent)	RA (percent)
75	190 - 196	228 - 250	11 - 15	13 - 18
1200	174 - 182	216 - 227	10 - 11	14 - 21

[a] Production of these parts included the following: -60 mesh argon-atomized powder; hot isostatically pressed (HIP) at 2175 - 2200F and 15 ksi, AC; forged 50 percent reduction at 2025F; semi-finish machined; heat treated (see Condition above); finish machined.

Table 3.3.1.5 Tensile properties at 1000F resulting from variations in atomizing gas, powder-mesh size, HIP cycle and heat treatment (Ref. 1)

Alloy	Rene 95						
Form	P/M HIP						
Mesh Size	HIP Cycle (F-hr)[a]	Aging Treatment (F-hr)[b]	Atomizing Gas	F_{ty} (ksi)	F_{tu} (ksi)	e (percent)	RA (percent)
-140	2200-3	1400-8	Argon	164.1	218.3	12.3	13.2
	2050-3	1400-8	Argon	172.8	234.7	14.2	15.0
-270	2200-3	1600-1 + 1200-24	Argon	160.1	219.4	12.2	11.7
	2050-3	1600-1 + 1200-24	Argon	172.2	235.2	14.7	13.1
	2050-3	1600-1 + 1200-24	Helium	169.5	225.9	14.8	13.4

[a] HIP at 15 ksi.

[b] All compacts solution treated 1 hour at 2090F and quenched into 1000F salt prior to aging treatment.

Table 3.3.1.6 Tensile properties at 1000F resulting from variations in HIP cycle and heat treatment (Ref. 1)

Alloy	Rene 95					
Form	P/M HIP, -140 mesh					
HIP Cycle at 15 ksi (F-hr)	Solution treatment[a] (F-hr)	Aging Treatment (F-hr)	F_{ty} (ksi)	F_{tu} (ksi)	e (percent)	RA (percent)
1800-10[b]	2090-1	1600-1 + 1200-24	176.0	232.5	12.6	10.0
1925-7	2090-1	1600-1 + 1200-24	175.4	227.5	10.6	9.0
	2090-1	1400-8	174.3	235.1	14.7	16.8
2050-3	2000-1	1600-1 + 1200-24	165.3	225.9	16.7	15.2
	2090-1	1600-1 + 1200-24	172.8	224.9	10.4	8.2
	2175-1	1600-1 + 1200-24	165.5	216.0	10.3	9.4
2175-3	2090-1	1600-1 + 1200-24	—[c]	206.2	8.3	7.0
	2175-1 + 2090-1	1600-1 + 1200-24	166.1	212.0	9.2	8.2

[a] Following solution treatment, all materials were quenched into 1000F salt.

[b] Last three hours at 30 ksi.

[c] Extensometer malfunctioned.

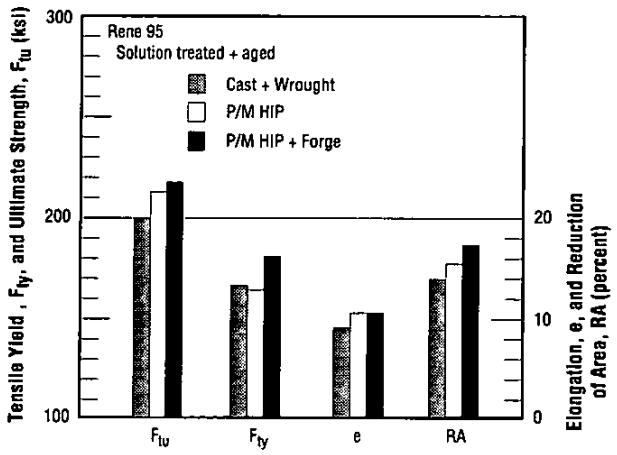

Figure 3.3.1.7 Tensile properties at 1200F resulting from various forming methods (Ref. 24)

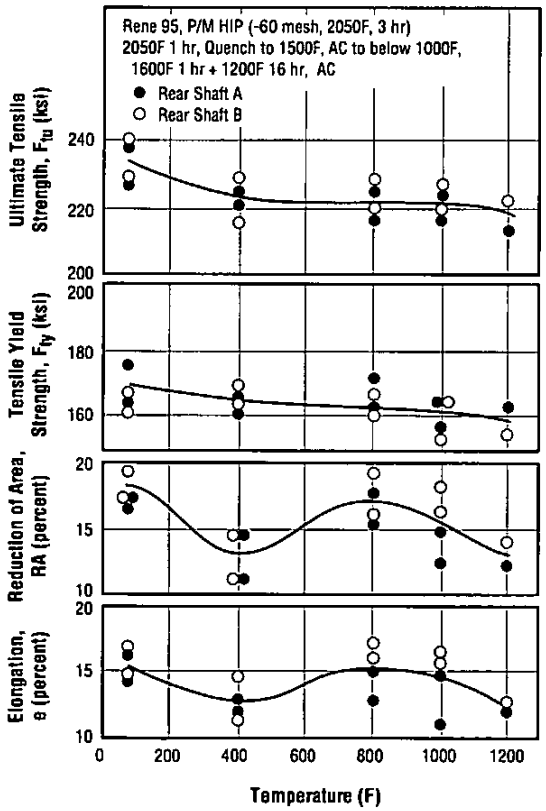

Figure 3.3.1.8 Effects of elevated temperatures up to 1200F on tensile properties of two rear shafts (Ref. 30)

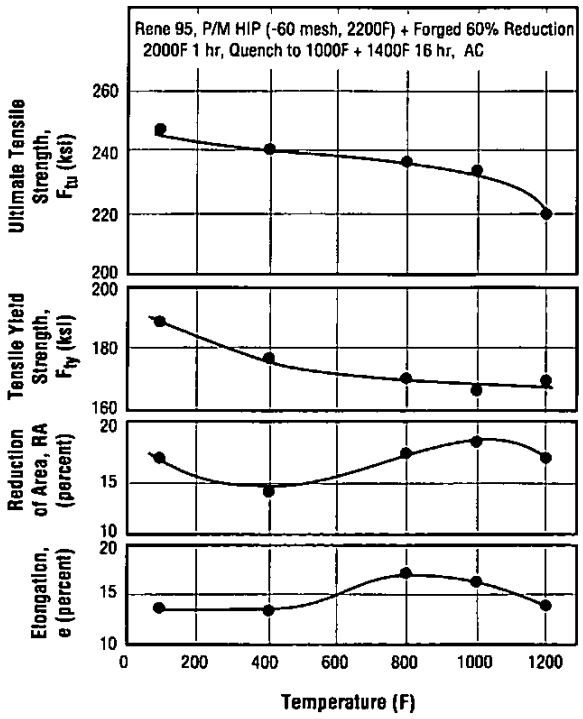

Figure 3.3.1.9 Effects of elevated temperatures up to 1200F on tensile properties of compressor discs (Ref. 30)

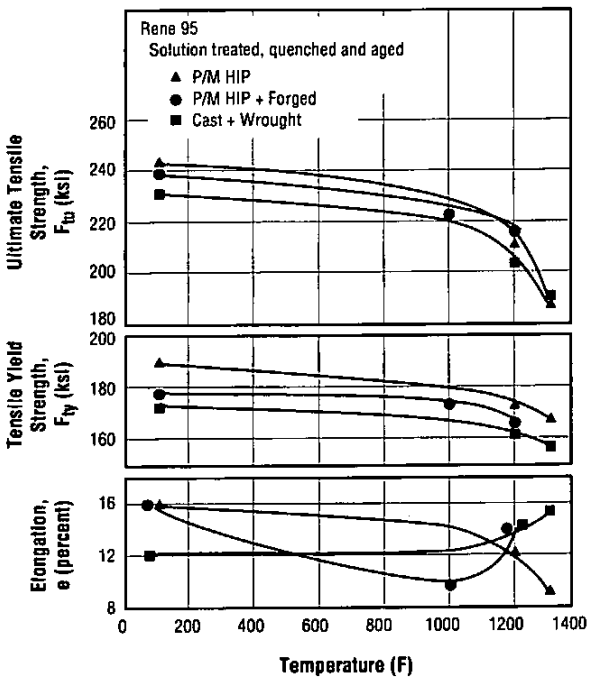

Figure 3.3.1.10 Effects of different production processes on tensile properties at temperatures up to 1400F (Ref. 10)

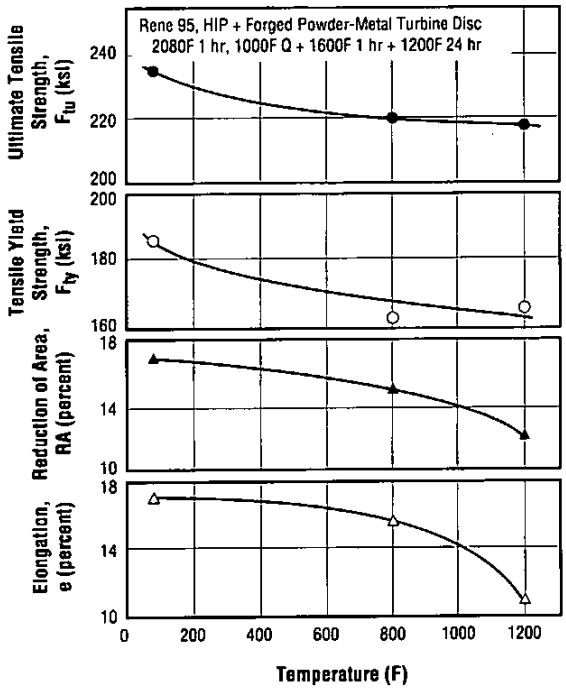

Figure 3.3.1.11 Effects of elevated temperatures up to 1200F on tensile properties of turbine disc (Ref. 9)

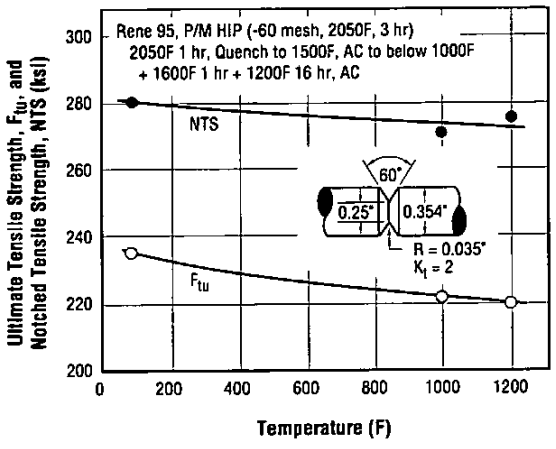

Figure 3.3.7.1.1 Comparison of ultimate tensile strength and notched tensile strength (K_t = 2) of rear shafts at temperatures up to 1200F (Ref. 30)

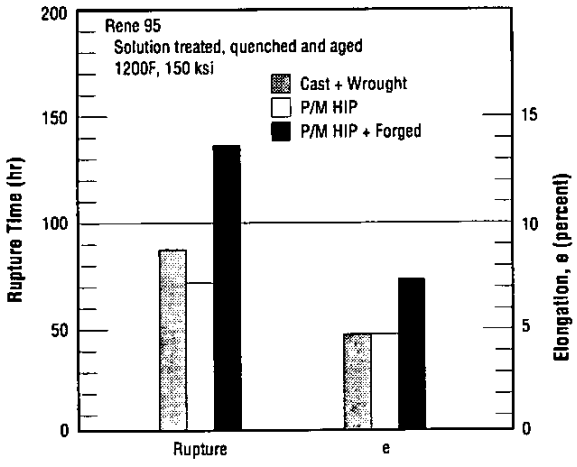

Figure 3.4.1 Stress-rupture properties at 1200F and 150 ksi of Rene 95 formed by various methods (Ref. 24)

Table 3.4.2 Mean results of stress-rupture and creep tests on specimens from 150 P/M HIP jet-engine discs (Ref. 14)

Alloy	Rene 95
Form	P/M HIP Jet-Engine Discs
Condition	Solution Treated, Quenched and Aged
Stress-rupture Tests at 1200F and 150 ksi	
Mean Rupture Time (hr)	88.8
Standard Deviation	26.3
Mean Elongation (percent)	6.5
Standard Deviation	2.1
Creep Tests at 1100F and 150 ksi	
Mean Time to 0.1% Elongation (hr)	54.6
Standard Deviation	6.7

Table 3.4.3 Stress-rupture life of six HIP plus forged powder products (2 tests each) at 1200F and 150 ksi (Ref. 3)

Alloy	Rene 95	
Form	P/M HIP Plus Forged Powder Products	
Condition	1650F 24 hr, AC + 2000F 1 hr, OQ + 1400F 16 hr, AC	
Part [a]	Rupture Time (hr)	e (percent)
Turbine Disc No. 1	195 167	5 7
Turbine Disc No. 2	134 124	5 9
Cooling Plate No. 1	185 150	9 10
Cooling Plate No. 2	253 311	7 7
Cooling Plate No. 3	187 198	5 6
Cooling Plate No. 4	140 150	10 9

[a] Production of these parts included the following: -60 mesh atomized powder, hot isostatically pressed (HIP) at 2175 - 2200F and 15 ksi, AC; forged 50 percent reduction at 2025F; semi-finish machined; heat treated (see Condition above); finish machined.

Table 3.4.4 Creep-rupture properties of forgings at 1200F (Refs. 15, 29)

Alloy	Rene 95	
Form	Cast + Forged	
Condition	2000F 1 hr, OQ + 1400F 16 hr, AC	
Stress (ksi)	Secondary Creep Rate (in./in./min)	Failure Time (hr)
180	5.26×10^{-4}	1.57
171	5.88×10^{-5}	7.22
160	4.00×10^{-5}	16.0

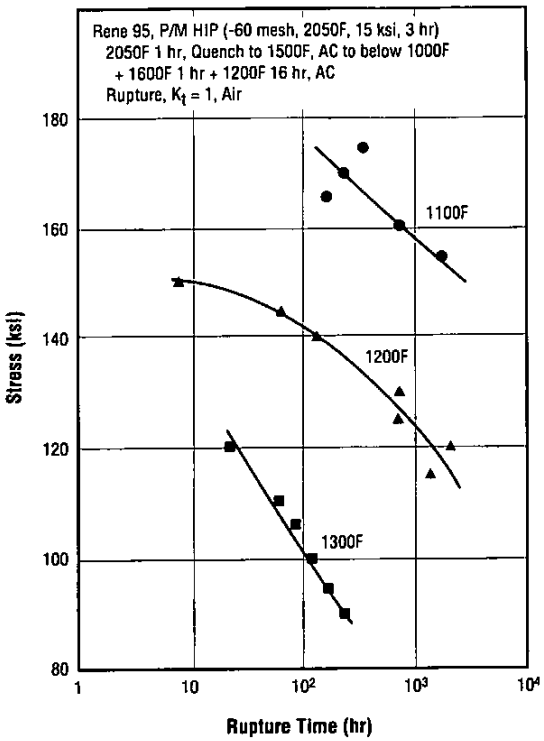

Figure 3.4.5 Stress-rupture properties of rear shafts at 1100 to 1300F (Ref. 30)

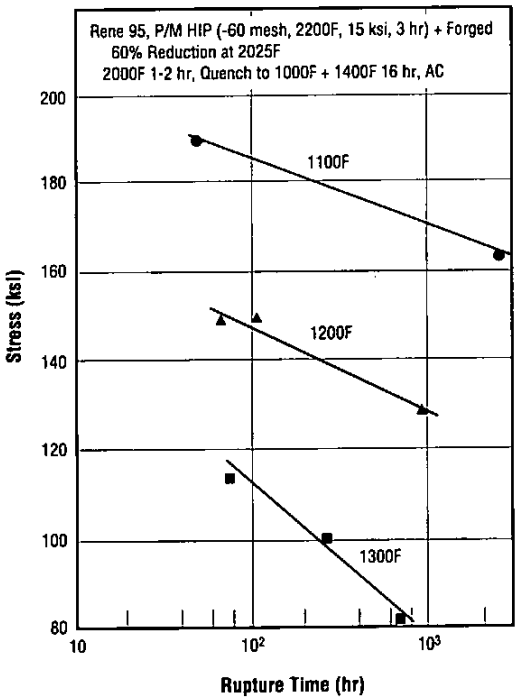

Figure 3.4.6 Stress-rupture properties of compressor discs at 1100 to 1300F (Ref. 30)

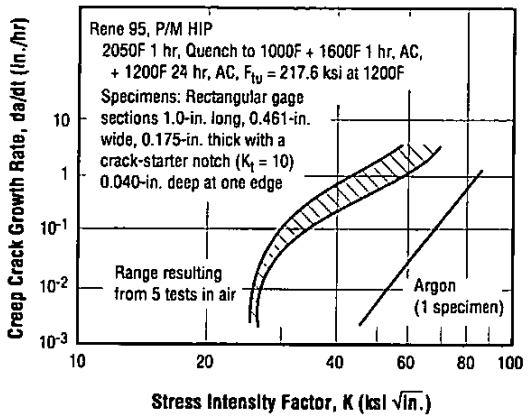

Figure 3.4.7 Creep crack growth rate as a function of stress intensity factor at 1200F in air and in purified argon (Ref. 6)

Note: In these tests, the creep-rupture times ranged from 3.2 hours up to 102.4 hours, each of which consisted of a time for creep-crack initiation plus a time for creep-crack growth to failure. The time for crack initiation varied from 90 percent of the shortest rupture up to 99 percent of the longest rupture time, whereas the corresponding crack-growth times varied from 10 percent to only 1 percent of the total rupture times.

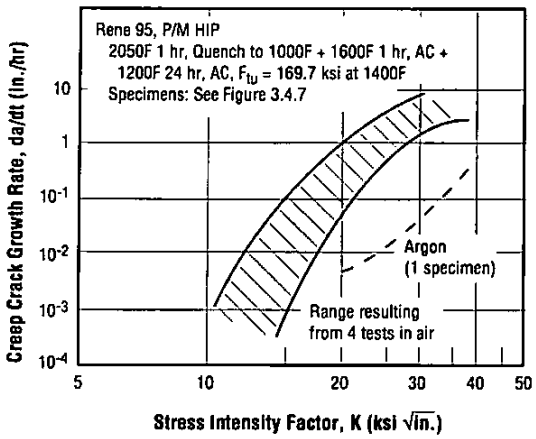

Figure 3.4.8 Creep crack growth rate as a function of stress intensity factor at 1400F in air and in purified argon (Ref. 6)

Note: In these tests, the creep-rupture times ranged from 6.5 hours up to 33.6 hours, each of which consisted of a time for creep-crack initiation plus a time for creep-crack growth to failure. The time for crack initiation varied from 88 percent of the shortest rupture up to 99 percent of the longest rupture time, whereas the corresponding crack-growth times varied from 12 percent to only 1 percent of the total rupture times.

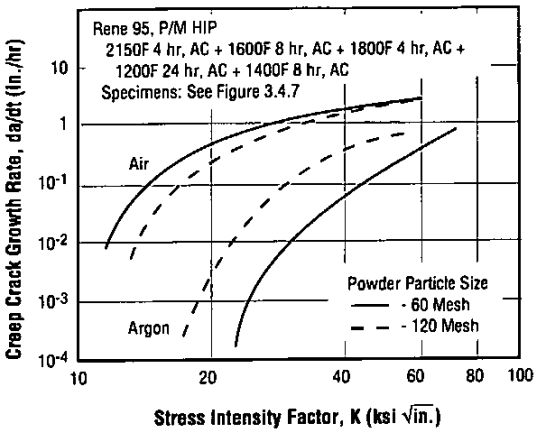

Figure 3.4.9 Creep crack growth rate as a function of stress intensity factor at 1300F in air and in purified argon (Ref. 28)

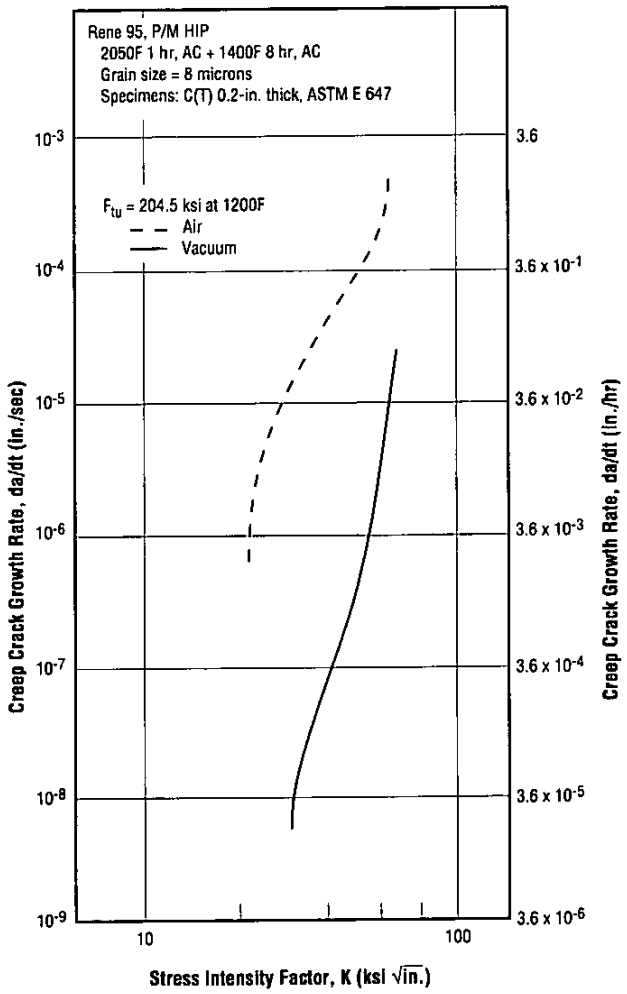

Figure 3.4.10 Creep crack growth rate as a function of stress intensity factor at 1200F in air and in vacuum (Ref. 21)

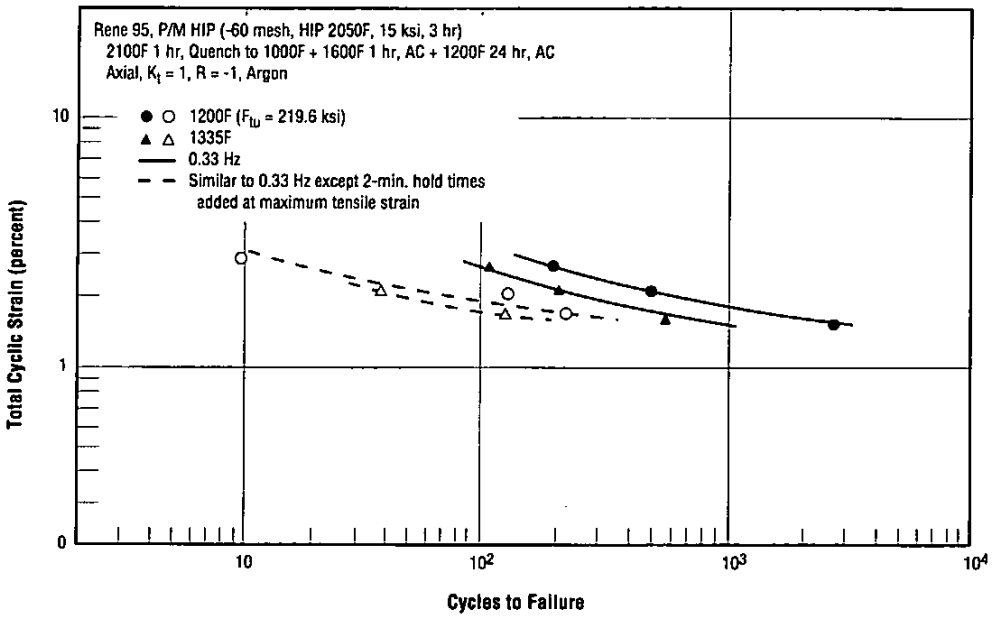

Figure 3.5.2.1 Effects of holding two minutes at maximum cyclic tensile strain on low-cycle fatigue life of P/M HIP Rene 95 as a function of total cyclic strain at 1200 and 1325F in argon (Refs. 5, 7, 27)

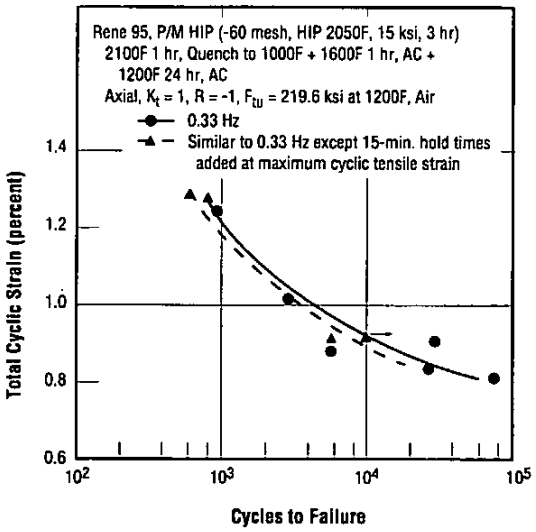

Figure 3.5.2.2 Effects of holding 15 minutes at maximum cyclic tensile strain on low-cycle fatigue life of P/M HIP Rene 95 as a function of total cyclic strain at 1200F in air (Refs. 26, 32)

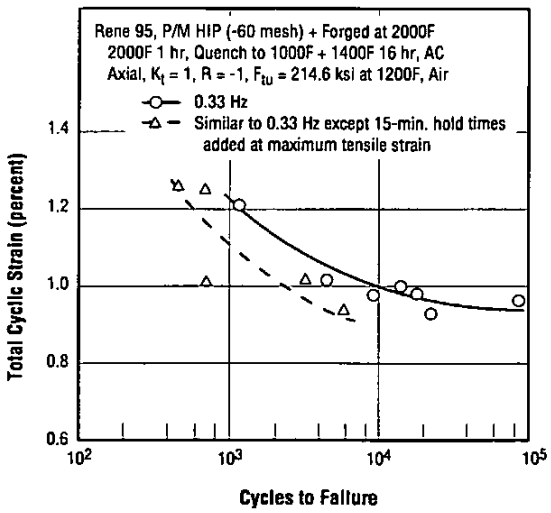

Figure 3.5.2.3 Effects of holding 15 minutes at maximum cyclic tensile strain on low-cycle fatigue life of P/M HIP plus forged Rene 95 as a function of total cyclic strain at 1200F in air (Refs. 26, 32)

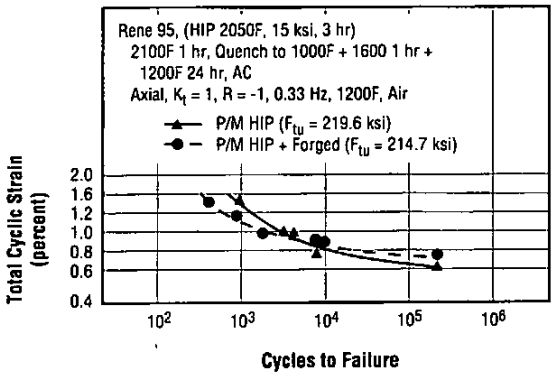

Figure 3.5.2.4 Low-cycle fatigue life at 1200F as a function of total cyclic strain for HIP and HIP plus forged Rene 95 (Ref. 18)

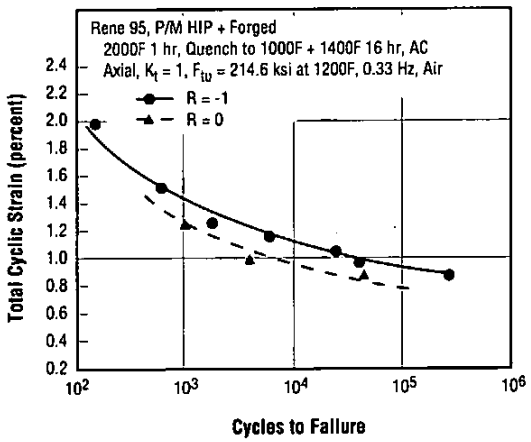

Figure 3.5.2.5 Low-cycle fatigue life of HIP plus forged Rene 95 as a function of total cyclic strain at 1200F with two different strain ratios (minimum cyclic strain/maximum cyclic strain) (Ref. 33)

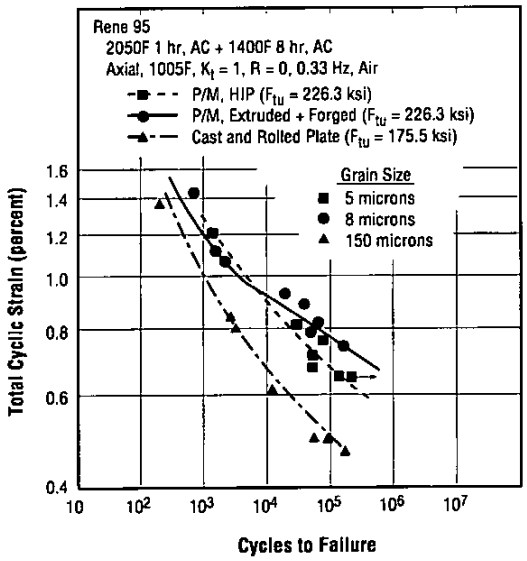

Figure 3.5.2.6 Effects of different forming methods on low-cycle fatigue life as a function of total cyclic strain at 1005F (Ref. 16)

Note: Prior to solution-and-age heat treatment, the wrought plate was homogenized at 2225F one hour and air cooled.

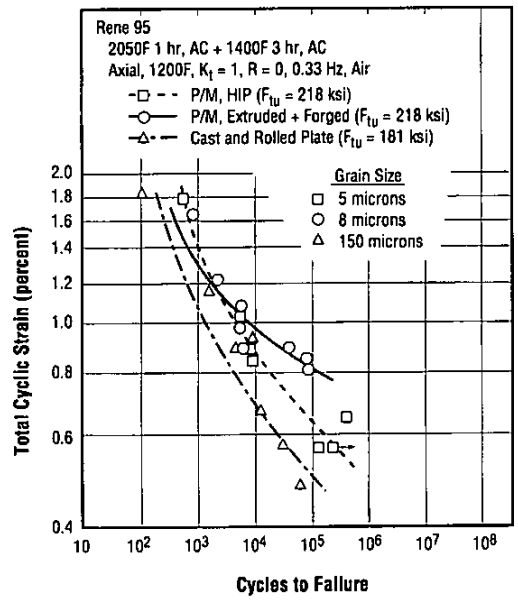

Figure 3.5.2.7 Effects of different forming methods on low-cycle fatigue life as a function of total cyclic strain at 1200F (Ref. 16)

Note: Prior to solution-and-age heat treatment, the wrought plate was homogenized at 2225F one hour and air cooled.

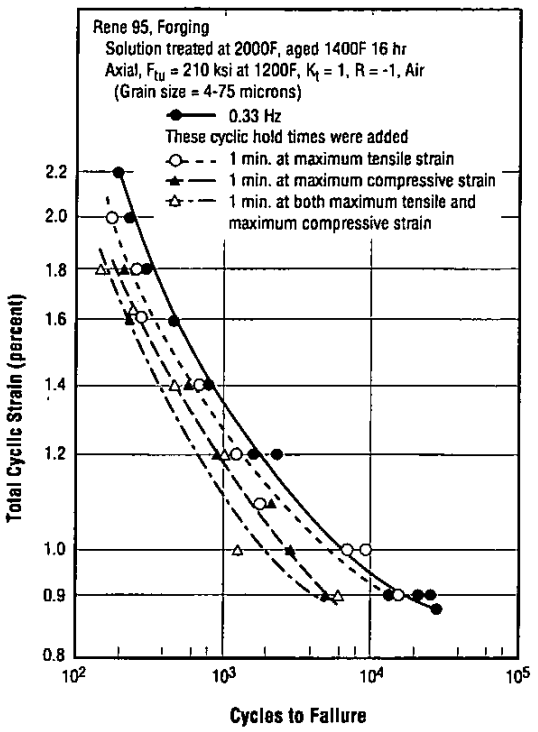

Figure 3.5.2.8 Effects of variations in cyclic hold times on the low-cycle fatigue life of forgings as a function of total cyclic strain at 1200F (Refs. 17, 29)

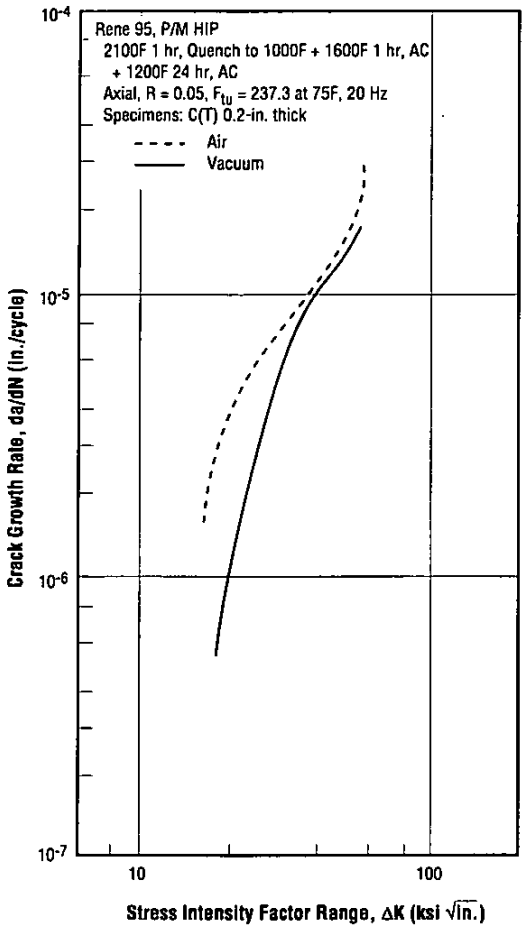

Figure 3.5.3.1 Fatigue crack growth rates at room temperature in air and in vacuum (Refs. 7, 8)

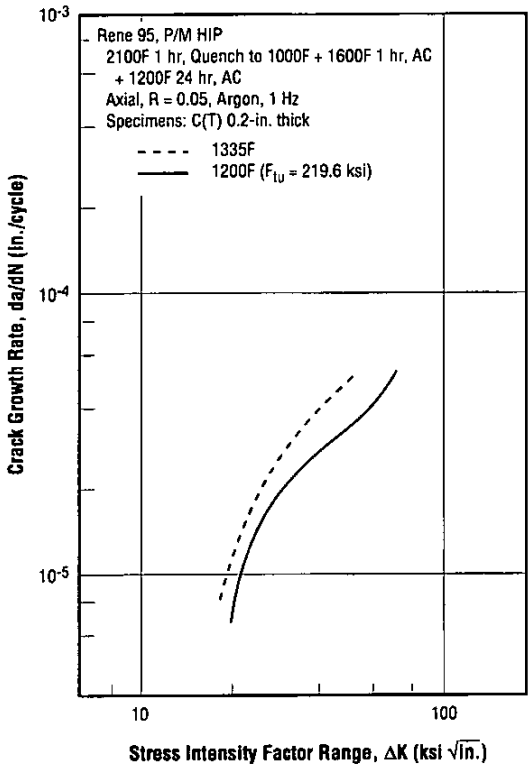

Figure 3.5.3.2 Fatigue crack growth rates at 1200F and 1335F in argon (Refs. 7, 8)

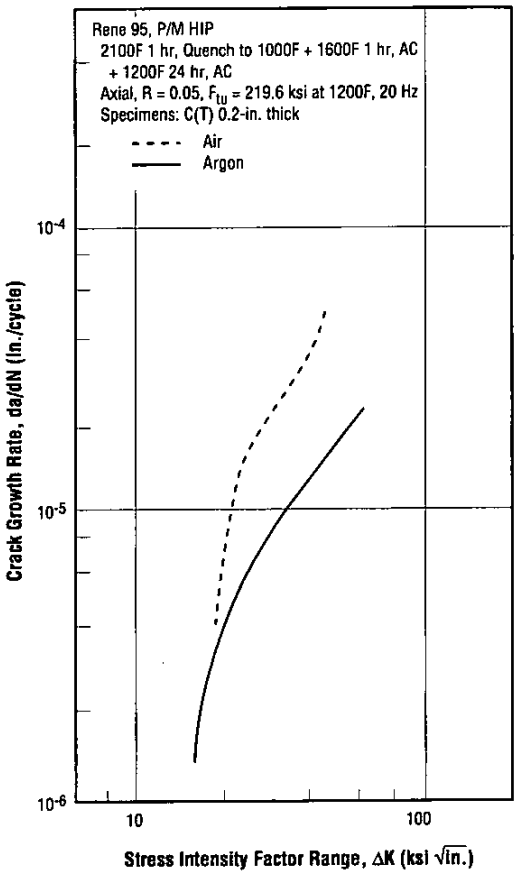

Figure 3.5.3.3 Fatigue crack growth rates at 1200F in air and in argon (Refs. 7, 8)

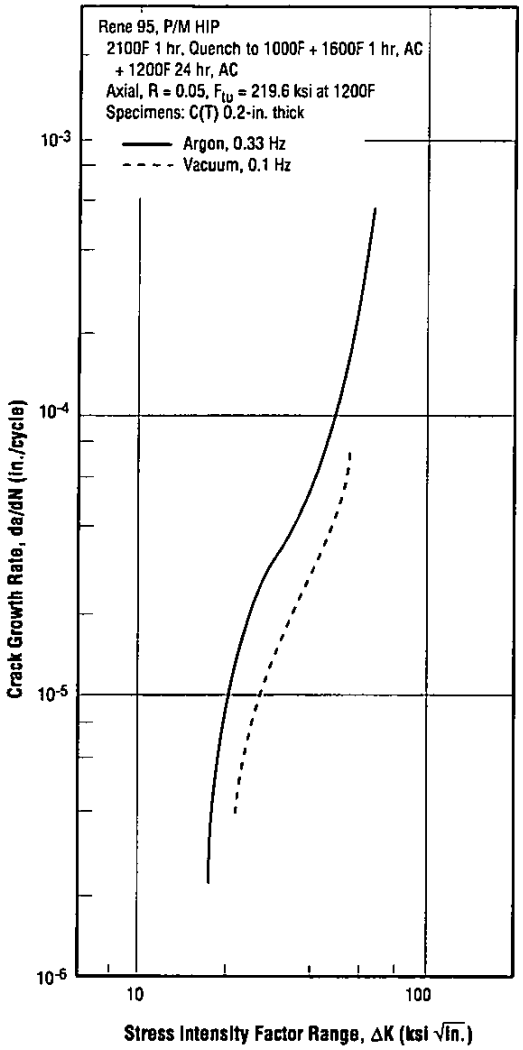

Figure 3.5.3.4 Fatigue crack growth rates at 1200F in vacuum and in argon (Refs. 5, 7, 8)

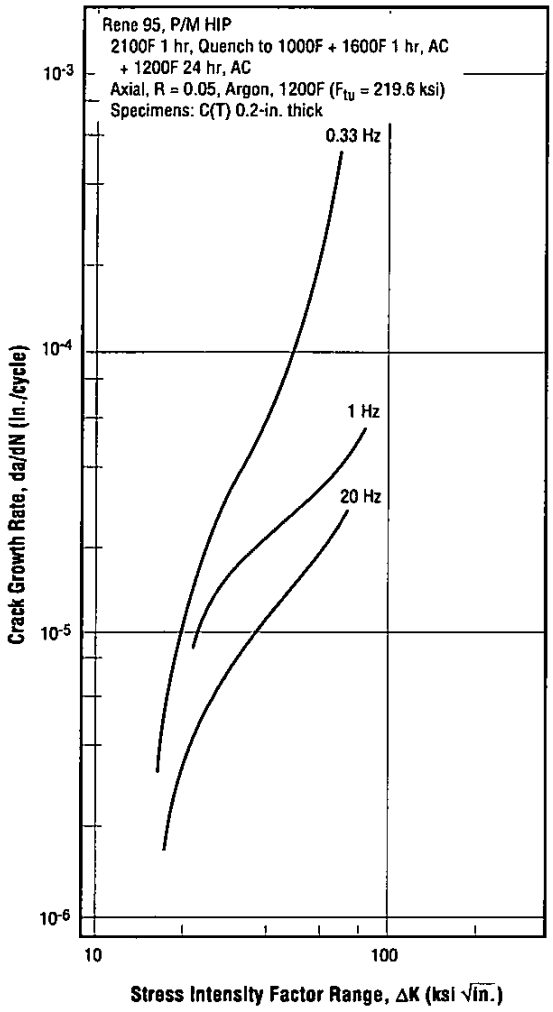

Figure 3.5.3.5 Effects of variations in cycling rate on fatigue crack growth rates at 1200F in argon (Refs. 5, 7, 8)

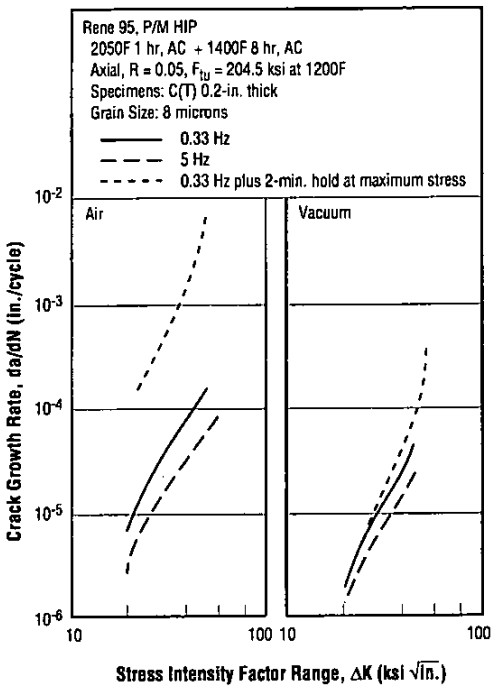

Figure 3.5.3.6 Effects of variations in cycling rate on fatigue crack growth rates at 1200F in air and in vacuum (Ref. 21)

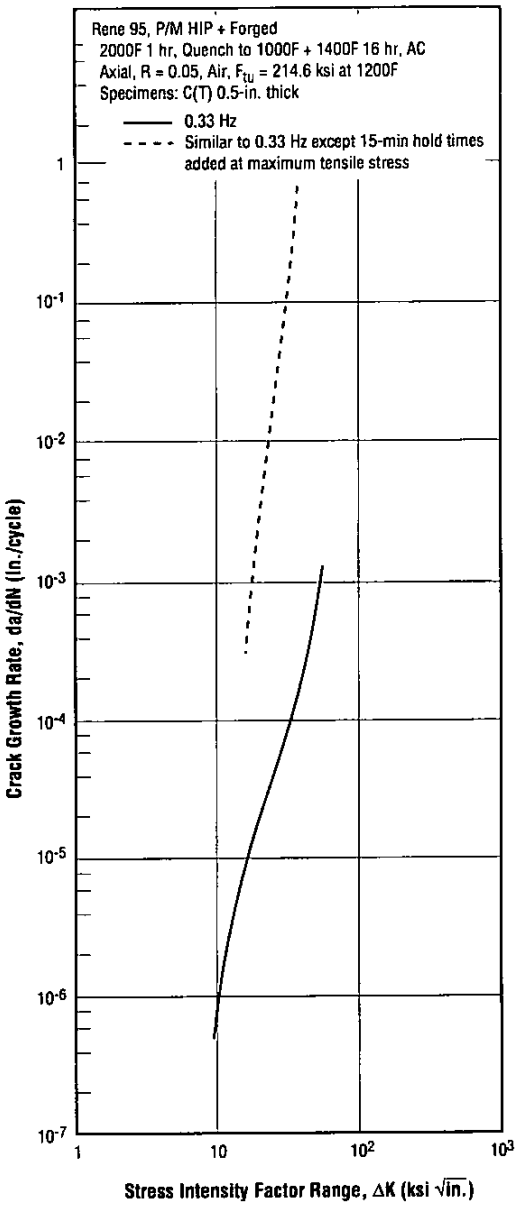

Figure 3.5.3.7 Effects of holding 15 minutes at maximum cyclic tensile stress on the fatigue crack growth rates at 1200F in air (Ref. 33)

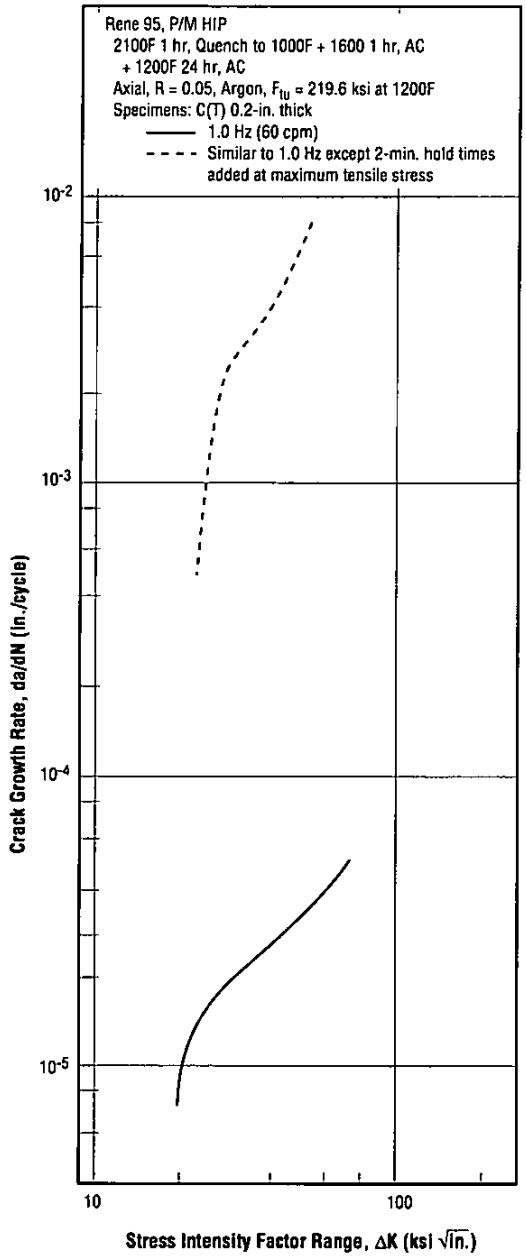

Figure 3.5.3.8 Effects of holding two minutes at maximum cyclic tensile stress on the fatigue crack growth rates at 1200F in argon (Refs. 5, 7, 8)

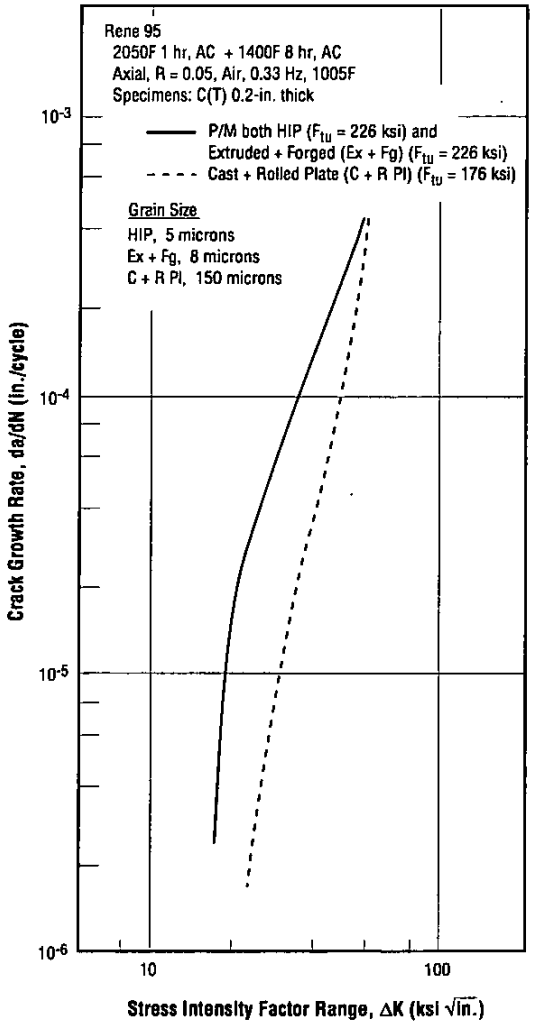

Figure 3.5.3.9 Effects of different forming methods and grain sizes on fatigue crack growth rates at 1005F in air at 0.33 Hz (Ref. 16)

Note: Prior to the solution-and-age heat treatment, the wrought plate was homogenized at 2225F one hour and air cooled.

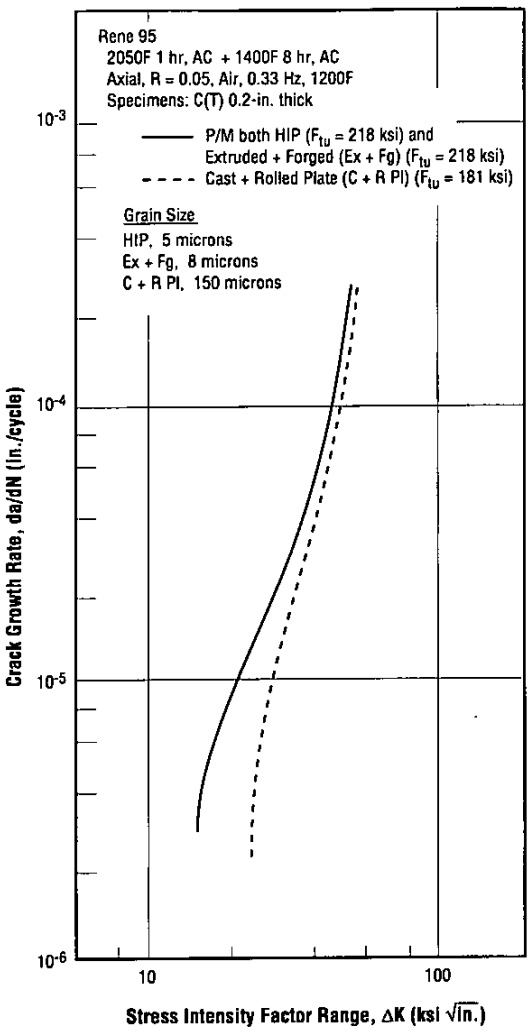

Figure 3.5.3.10 Effects of different forming methods and grain sizes on fatigue crack growth rates at 1200F in air at 0.33 Hz (Ref. 16)

Note: Prior to the solution-and-age heat treatment, the wrought plate was homogenized at 2225F one hour and air cooled.

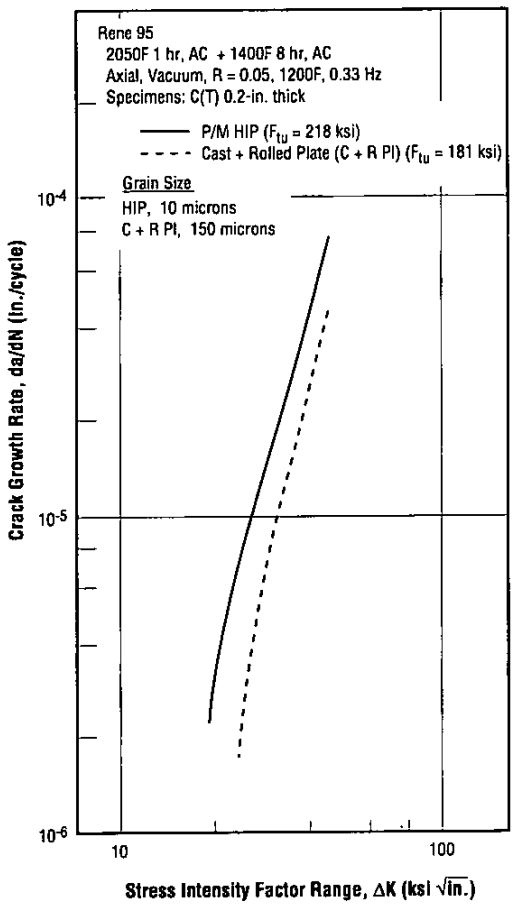

Figure 3.5.3.11 Effects of different forming methods and grain sizes on fatigue crack growth rates at 1200F in vacuum at 0.33 Hz (Ref. 22)

Note: Prior to the solution-and-age heat treatment, the wrought plate was homogenized at 2225F one hour and air cooled.

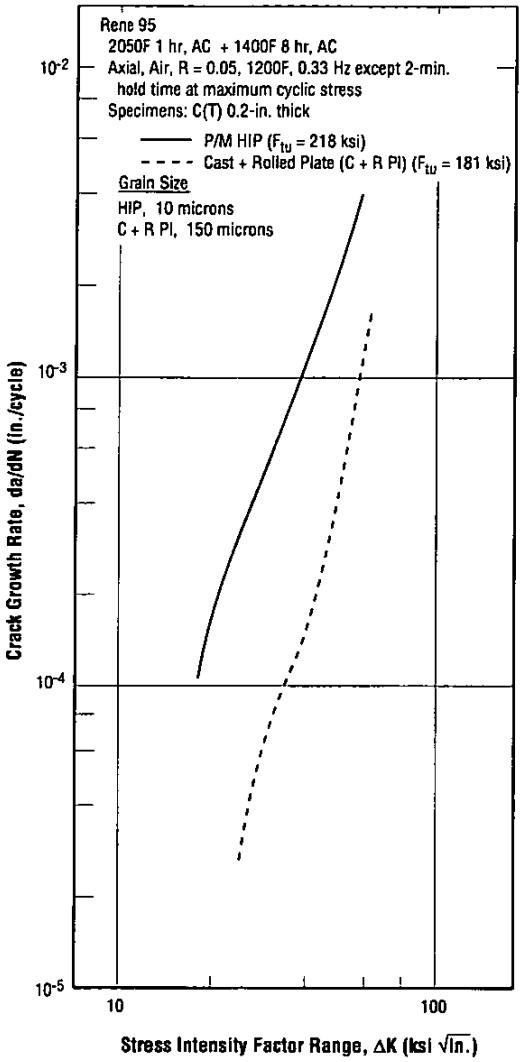

Figure 3.5.3.12 Effects of different forming methods and grain sizes on fatigue crack growth rates at 1200F in air with cycling at 0.33 Hz plus 2-minute hold times at maximum cyclic stress (Ref. 22)

Note: Prior to the solution-and-age heat treatment, the wrought plate was homogenized at 2225F one hour and air cooled.

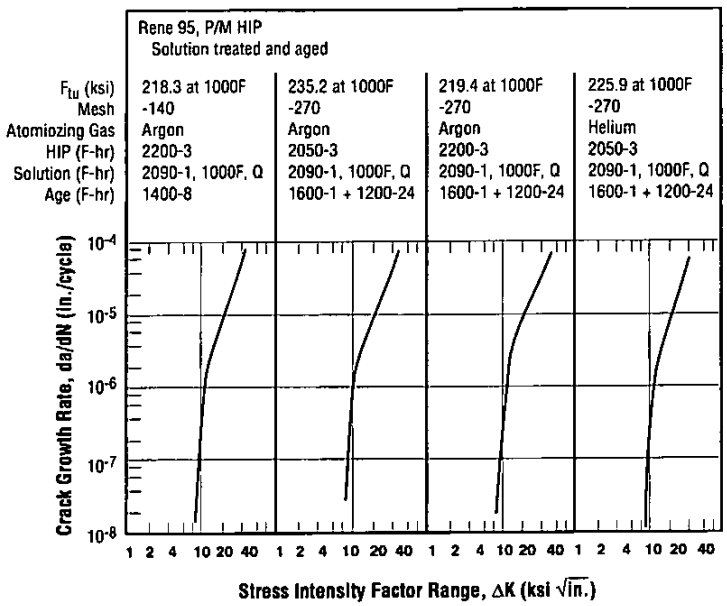

Figure 3.5.3.13 Effects of variations in powder mesh size and processing parameters on crack growth rates in axial fatigue at 1000F, 0.33 Hz and R = 0.05, in air.

Note: Specimens were hour-glass shape, 0.25-in. minimum diameter, with a sharp chord defect created by electrical-discharge machining (EDM) (Ref. 1)

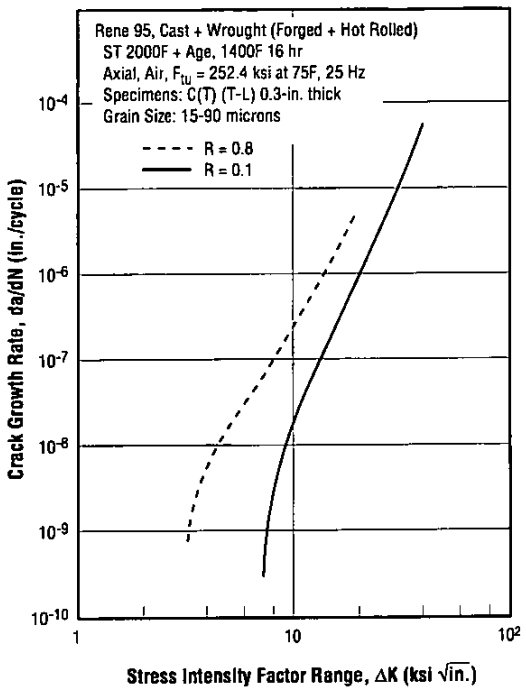

Figure 3.5.3.14 Effects of different R values (min/max cyclic stress) on near threshold fatigue crack growth rates of wrought Rene 95 at 75F in air at 25 Hz (Ref. 20)

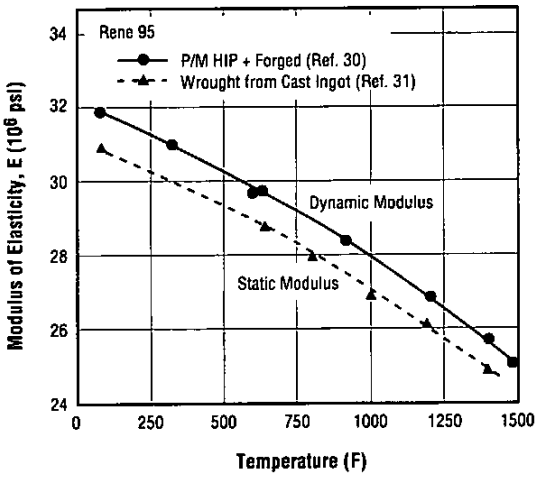

Figure 3.6.2.1 Modulus of elasticity at temperatures from 75F to 1500F (Refs. 30, 31)

References

1. Van Stone, R.H., and Gangloff, R.P., "The Effect of Processing Parameters on the Microstructure and Mechanical Properties of Rene 95 Consolidated from Gas Atomized Powders," *Proceedings of the Second International Conference on Rapid Solidification Processing*, pp. 317-330 (March 1990).
2. Bartos, J.L, Allen, R.E., Thompson, V.R., Moss, J.H., and Morris, C.A., "Development of Hot-Isostatically Pressed and Forged P/M Rene 95 for Turbine Disc Application," SAE, National Aerospace Engineering and Manufacturing Meeting, San Diego, CA (October 1974).
3. ASM Metals Handbook, Ninth Edition, Vol. 7, *Powder Metallurgy*, p. 441 (1984).
4. Happ, M.B., and San Clemente, P., "HIP of Rene 95," *U.S. Army ManTech Journal*, Vol. 4.4, pp. 41-44 (1979).
5. Stoloff, N.S., Duquette, D.J., Choe, S.J., and Golwalkar, S.V., "Fatigue Crack Growth and Low-Cycle Fatigue of Two Nickel-Base Superalloys," Rensselaer Polytechnic Institute, Report No. N84-10267 (September 1983).
6. Bain, K.R., and Pelloux, R.M., "Effect of Environment on Creep Crack Growth in PM/HIP Rene 95," *Metallurgical Transactions*, Vol. 15A:2, pp. 381-388 (February 1984).
7. Choe, S.J., "High Temperature Low Cycle Fatigue and Correlation to Crack Growth Rate in Two Nickel Base Superalloys," Graduate Thesis, Rensselaer Polytechnic Institute (November 1985).
8. Golwalker, S.V, "Creep-Fatigue-Environmental Interactions in Ni-Base Superalloys," Graduate Thesis, Rensselaer Polytechnic Institute (August 1984).
9. Mathur, P.S., and Bartos, J.L., "Development of Hot Isostatically Pressed Rene 95 Turbine Parts," USARTL-TR-78-56, U.S. Army Research and Technology Laboratories, Fort Eustis, VA (April 1979).
10. Thompson, E.R., "High Temperature Aerospace Materials Prepared by Powder Metallurgy," *Annual Review of Material Sciences*, Vol. 12, pp. 213-242 (1982).
11. Fu, Z.M., Au, P., Morphy, D., Koul, A.K., and Immarigeon, J.P., "Influences of Microstructure on High Temperature Low-Cycle Fatigue Life in P/M Rene 95," *Conference on Mechanical Behavior of Materials*, Vol. 2, Beijing, China (3-6 June 1987).
12. Shamblen, C.E., and Chang, D.R., "Effect of Inclusions on LCF Life of HIP Plus Heat Treated Powder Metal Rene 95," *Metallurgical Transactions*, Vol. 16:B4, pp. 775-784 (December 1984).
13. Bashir, S., Taupin, P., and Antolovich, S.D., "Low-Cycle Fatigue of As-HIP and HIP + Forged Rene 95," *Metallurgical Transactions A*, Vol. 10A, pp. 1481-1490 (October 1979).
14. Dulis, E.J., Moll, J.H., Chandhok, V.K., and Hebseisen, J.C., "Progress in P/M Superalloy and Titanium for Aircraft Applications," *Proceedings of the 25th National SAMPE Symposium and Exhibition*, pp. 75-89 (May 1980).
15. Hyzak, J.M., and Bernstein, H.L., "An Analysis of the Low Cycle Fatigue Behavior of the Superalloy Rene 95 by Strainrange Partitioning," Air Force Materials Laboratory, TR-78-174 (November 1978).
16. Miner, R.V., and Gayda, J., "Effects of Processing and Microstructure on the Fatigue Behavior of the Nickel-Base Superalloy Rene 95," *International Journal of Fatigue*, Vol. 6, No. 3, pp. 189-193 (July 1984).
17 Chin-I.S., "High Temperature Low Cycle Fatigue Mechanisms for a Nickel-Base and a Copper-Base Alloy," University of Cincinnati, NASA Contractor Report 3543 (1982).
18. Dreshfield, R.L., and Miner, R.V., "Application of Superalloy Powder Metallurgy for Aircraft Engines," NASA Technical Memorandum 81466, Lewis Research Center (June 1980).
19. Miner, R.V., Gayda, J., and Maier, R.D., "Creep and Creep-Fatigue Deformation of Several Nickel-Base Superalloys at 650F," *Metallurgical Transactions A*, Vol. 13A, pp. 1755-1765 (October 1982).
20. McCarver, J.F., and Ritchie, R.O., "Fatigue Crack Propagation Thresholds for Long and Short Cracks in Rene 95 Nickel-Base Superalloys," *Materials Science and Engineering*, Vol. 55:1, pp. 63-67 (August 1982).
21. Gayda, J, Gabb, T.P., and Miner, R.V., "Fatigue Crack Propagation of Nickel Superalloys at 650C," NASA Technical Memorandum 37150, NASA Lewis Research Center (1985).
22. Gayda, J., Miner, R.V., and Gabb, T.P., "On the Fatigue Crack Propagation Behavior of Superalloys at Intermediate Temperatures," *Conference: Superalloys 1984*, The Metallurgical Society AIME (October 1984).
23. Gayda, J., and Miner, R.V., "Fatigue Crack Initiation and Propagation in Several Nickel-Base Superalloys at 650C," *International Journal of Fatigue*, Vol. 5:3, pp. 135-143 (July 1983).
24. Tien, J.K., and Howison, T.E., "Advances in P/M and ODS Superalloys," *Proceedings of the 1981 ASM Materials Science Seminar, Advances in Powder Technology* (October 1981).
25. Chang, D.R., Krueger, D.D., and Sprague, R.A., "Superalloy Powder Processing, Properties, and Turbine Disc Applications," *Proceedings of the Fifth International Symposium in Superalloys 1994*, Metallurgical Society AIME (October 1984).

26. Bashir, S, "High Temperature Low-Cycle Fatigue of Nickel Base Superalloys," Graduate Thesis, University of Cincinnati (1982).

27. Choe, S.J., Golwalker, S.V., Duquette, D.J., and Stoloff, N.S., "The Influence of Hold Times on LCF and FCG Behavior in a P/M Ni-Base Superalloy," *Proceedings of the Fifth International Symposium on Superalloys* (October 1984).

28. Bain, K.R., and Pelloux, R.M., "Effect of Oxygen on Creep Crack Growth in P/M HIP Nickel-Base Superalloys," *Proceedings of the Fifth International Symposium on Superalloys* (October 1984).

29. Conway, J.B., and Stentz, R.H., "High-Temperature Low-Cycle Fatigue Data for Three High Strength Nickel-Base Superalloys," Air Force Systems Command AFWAL-TR-80-4077 (June 1980).

30. Pfouts, W.R., Shamblen, J.S., Mosier, J.S., Peebles, R.E., and Gorsler, R.W., "Powder Metallurgy Rene 95 Rotating Turbine Engine Parts," Vol. 1, General Electric Company, Report to NASA (CR-159802) (June 1979).

31. "Rene 95 Alloy," *Alloy Digest*, Filing Code Ni-203 (April 1974).

32. Shahani, V., and Popp, H.G., "Evaluation of the Cyclic Behavior of Aircraft Turbine Disc Alloys," General Electric Company, Report to NASA (CR-159433) (June 1978).

33. Cowles, B.A., Warren, J.R., and Haake, F.K., "Evaluation of the Cyclic Behavior of Aircraft Turbine Disc Alloys, Part II," Pratt and Whitney Company, Report to NASA (CR-165123) (July 1980).

34. McIntyre, R.D., "Superalloys More Super Than Ever," *Materials Engineering*, Vol. 95, pp. 36-43 (January 1982).

35. ASTM E 112-88, "Standard Test Methods for Determining Average Grain Size," ASTM Vol. 301 (1992).

36. Chenggong, L., Lian, J., Liu, J., and Wang. Z., "The Deformation Behavior of HIP P/M Rene 95 Superalloy Under Isothermal Upsetting," *First Pacific Rim International Conference on Advanced Materials and Processing*, Haugzhow China (June 1992).

This page is blank.